Talanta 121 (2014) 144–152

Contents lists available at ScienceDirect

Talanta

journal homepage: www.elsevier.com/locate/talanta

Determination of fat and total protein content in milk using conventional digital imaging

Sergey Kucheryavskiy [a,*], Anastasiia Melenteva [b], Andrey Bogomolov [b,c]

[a] Section of Chemical Engineering, Aalborg University, Campus Esbjerg, Niels Bohrs vej, 8, Esbjerg 6700, Denmark
[b] Samara State Technical University, Samara, Russia
[c] J&M Analytik AG, Essingen, Germany

ARTICLE INFO

Article history:
Received 27 July 2013
Received in revised form
3 December 2013
Accepted 24 December 2013
Available online 3 January 2014

Keywords:
Milk quality
Digital imaging
Image analysis
Light scatter

ABSTRACT

The applicability of conventional digital imaging to quantitative determination of fat and total protein in cow's milk, based on the phenomenon of light scatter, has been proved. A new algorithm for extracting features from digital images of milk samples has been developed. The algorithm takes into account spatial distribution of light, diffusely transmitted through a sample.

The proposed method has been tested on two sample sets prepared from industrial raw milk standards, with variable fat and protein content. Partial Least-Squares (PLS) regression on the features calculated from images of monochromatically illuminated milk samples resulted in models with high prediction performance when analysed the sets separately (best models with cross-validated $R^2=0.974$ for protein and $R^2=0.973$ for fat content).

However when analysed the sets jointly with the obtained results were significantly worse (best models with cross-validated $R^2=0.890$ for fat content and $R^2=0.720$ for protein content). The results have been compared with previously published Vis/SW-NIR spectroscopic study of similar samples.

1. Introduction

Efficient routine analysis of milk quality is of critical importance for any dairy production. Fat and protein content are two particularly important milk quality parameters, characterising its nutritional value. Nowadays, traditional physicochemical analysis of milk tends to be replaced by modern optical spectroscopic techniques combined with multivariate data analysis. Thus, mid-infrared spectroscopy has been widely accepted as a laboratory standard for the milk nutrient analysis [1]. At the same time, constantly growing demand for real-time milk analysis stimulates the development of alternative techniques capable of performing in-line or field measurements. An effective real-time technique should provide high throughput and reliability of analysis at a reasonable price.

The present work gives further development to the idea of exploiting the phenomenon of light scattering by fat and protein particles for their quantitative analysis. Early turbidimetric analysis was based on the observed correlation between the fat content and the detected extinction of light dispersed by a milk sample at individual wavelengths [2,3]. This method, however, is highly susceptible to the size variability of colloidal milk particles, even in homogenised milk, and thus, is now considered obsolete. There are only a few later works making use of the scatter for milk fat and protein analysis. They typically require an intensive pretreatment of milk samples, i.e. deep homogenisation and protein dispersion [4], and thus, are impracticable in the case of raw natural milk. The light propagation in the raw milk also stays too complex for a direct theory-based solution, due to the presence of two species having complex and varying size distributions under the conditions of multiple scattering. As a consequence, optical spectroscopic methods of fat and protein determination are mainly based on the components' absorption, provided that the scatter is possibly avoided or suppressed [5]. The visible (Vis) light region (360–780 nm), where the scatter strongly dominates, is rarely used in quantitative milk analysis [6,7]. At the same time, the Vis region is very attractive for the analysis, because of a wide choice of available equipment, including light sources and guides, optics and detectors.

The feasibility of scatter-based quantitative analysis of fat and total protein in the raw milk using Vis and short-wave near infrared (SW-NIR) spectroscopy has been recently proved by Bogomolov et al. [8–10], the difference of individual spectral patterns (i.e. wavelength dependencies) of scatter by differently sized protein and fat particles was shown to be sufficient for their quantitative analysis using formal multivariate modelling, e.g. PLS regression. The method successfully handles an artificially introduced variation of fat globule sizes [8].

* Corresponding author. Tel.: +45 2787 9818.
E-mail address: svk@bio.aau.dk (S. Kucheryavskiy).

0039-9140/$ - see front matter © 2013 Elsevier B.V. All rights reserved.
http://dx.doi.org/10.1016/j.talanta.2013.12.055

The present study develops further the ideas of using light scatter effect for analysis of milk quality published in [8,9] and aims at the elaboration of a technologically simple approach to the quantitative analysis of raw milk fat and protein content, using light emitting diodes (LED) as monochromatic light sources and conventional digital RGB imaging as a detection technique. This combination, in fact, is an inexpensive alternative to optical spectroscopy. In this novel approach, an essential loss of spectral resolution is compensated by the detection area extension, thus, giving an advantage of detecting spatial intensity distribution of the scattered light.

Conventional digital imaging nowadays is increasingly used for quantitative analysis in industrial applications [11–13] but stays an uncommon tool for the milk analysis. The published work has been mainly devoted to a microscopic investigation of milk particles and their aggregates, e.g. [14–16]. To our knowledge, digital imaging has not been used for the quantitative analysis of milk constituents before. General feasibility of this approach was suggested in [17], where the opposite problem had been solved: rendering images of different media by their scatter and absorption properties using the Lorenz–Mie scattering theory generalisation.

This study presents the evaluation results of using conventional RGB digital imaging and light emitting diode (LED) illumination for quantitative determination of fat and total protein in raw milk. The modelling and validation is based on a designed experiment including the variability of fat globule sizes. Initially, intensity histograms, first-order statistics and Angle Measure Technique (AMT) have been tried as image features. Finally, a simple but efficient feature extraction algorithm, which takes into account spatial intensity distribution on the milk images, was developed. The PLS regression on features, calculated using the developed algorithm, gave models with practically relevant prediction performances confirming the feasibility of suggested approach. The results were compared with a recent Vis/SW-NIR spectroscopic study of the same sample set [8].

2. Materials and methods

2.1. Samples

The experimental samples were prepared from two sets of raw milk standards (QSE GmbH, Wolnzach, Germany) with predominantly varying fat or protein content – *F*- and *P*-set, respectively (Table 1). Sixteen samples were prepared from each set: four initial standards (with known fat and total protein content) and twelve their pair-wise mixtures in proportions 1:2 and 2:1. Every sample was analysed three times: in its original state and after two subsequent homogenisations: for 10 and 20 s, using an ultrasound homogeniser. The homogenisation was applied to introduce gentle variation of particle size distribution occurring in the natural milk and significantly affecting its scattering properties [10,18]. Sample homogenisation degree was qualitatively characterised by optical microscopy and Vis/SW-NIR spectroscopy [8]. Spectral changes caused by applied homogenisation times were comparable in magnitude with the effects fat and protein content differences in the chosen range, and therefore, presented an essential factor of sample variability.

Thereby each of the two sets was represented by three measurements (one for each homogenisation degree) of 16 samples, which gave 48 measurements per set (96 in total). Further information about the samples can be found in [8].

Table 1
Fat and total protein content in raw milk standards.

Sample	Fat, % w/w	Protein, % w/w
P1	3.63	2.99
P2	4.27	3.30
P3	4.03	3.71
P4	4.33	4.05
F1	1.99	3.45
F2	3.23	3.47
F3	4.22	3.61
F4	5.47	3.21

2.2. Image acquisition and preprocessing

Images were acquired with DSLR camera Canon 400D fixed on a tripod. For every measurement, 4 ml of milk was put into a Petri dish (inner diameter of 30 mm) placed in front of the camera so that the centre of the dish was coaxial with the lens optical axis. The thickness of milk layer in the dish was about 4 mm. Three powerful LEDs emitting blue (maximum intensity at 465 nm) green (526 nm), and red (630 nm) light, were used for sample illumination. The emission spectra of the diodes are shown in Fig. 1. The incident light was delivered through a fibre optical guide with 1.2 mm diameter, which was coaxially mounted at 90° to the to the Petri dish bottom. Thereby every image captured a LED light spot diffusely transmitted through the milk sample. The image acquisition was performed in a dark room at 24 ± 1 °C.

Five photos for each light source were taken using bracketing with exposition times of 1, 1/2, 1/4, 1/8, and 1/15 s. Therefore, every measurement was represented by 15 images. The acquired images were cropped automatically to remove the dish walls.

The cropping algorithm worked with grayscale representation of the images. For each image it found a light spot with maximum intensity using threshold segmentation, estimated the centre of the spot and cropped an image using equal distances from the centre, resulting in symmetric and easily comparable pictures. The final images had size of 1024×1024 pixels. Fig. 2 shows a full set of preprocessed images taken from one of the standards after 10 s of homogenisation.

The high dynamic range (HDR) images were also made for every bracketing series using an algorithm described in [19] and implemented in Matlab Image Processing Toolbox function *makehdr*. In this case every measurement was represented by three HDR images – one for each light source.

The purpose of using HDR images was twofold: to decrease the number of variables taking advantage of enhanced image dynamic range provided by the bracketing technique. HDR technique allows

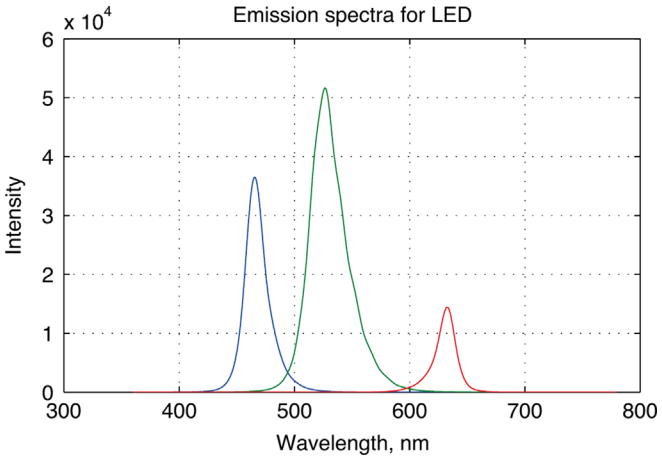

Fig. 1. Emission spectra of the used LEDs. (For interpretation of the references to color in this figure legend, the reader is referred to the web version of this article.)

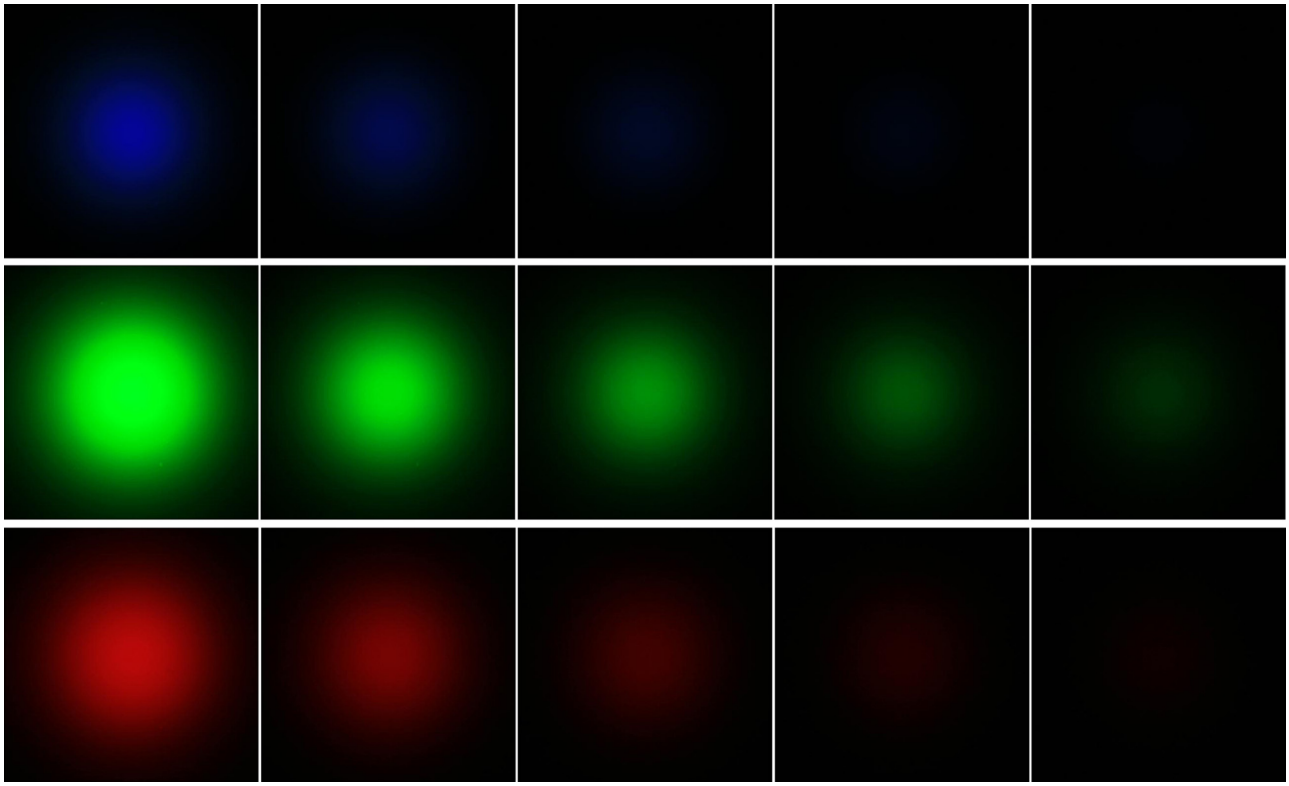

Fig. 2. A set of preprocessed images taken for the sample P1 (see Table 1) with exposition time: 1, 1/2, 1/4, 1/8, and 1/15 s.

capturing a larger dynamic range and represents intensity levels between the lightest and darkest part of image more accurate than the conventional imaging. In digital photography HDR images are typically used to improve the rendering and introduce various art effects. But the fact that it can emphasise small differences on an image can be also employed for analysis.

2.3. Extracting features

One of the simplest feature selection tools, operating on pixel intensities only, is the intensity distribution histogram. Elements of such histogram show fractions of image pixels having intensity within a particular range. In the standard digital imaging used in the present study, the pixel intensity varies from 0 (no light) to 255 (maximum intensity) so that the histogram has 256 values. It is also possible to reduce the detail by binning and calculating the histogram for selected intensity ranges. However, the histogram is an integral property of the whole image that does not retain any information on the spatial intensity distribution.

Another approach, specifically adjusted for the problem at hand, was based on a straightforward assumption that pixels equally distant from the illumination spot are supposed to be identical, and thus, can be averaged. Therefore, the image can be transformed into a radial intensity function that can be used for the selection of features with a necessary spatial resolution.

In accordance to this approach, an image is divided to $N=2^n$ concentric rings by using circles with radii: M/N, $2M/N$, $3M/N$, …, M, where M is a half of image width, in our case 512 pixels.

Then an average intensity of pixels with distance from the centre between XM/N and $(X+1)N/M$ (lying between circles with these radii) was calculated for every X from 0 to N–1. In order to do that, the image was transformed to a matrix with rows corresponding to the image pixels. The columns of the matrix included the pixels coordinates, intensity, and distance to the image centre, so the proper subset could be easily selected using logical expressions.

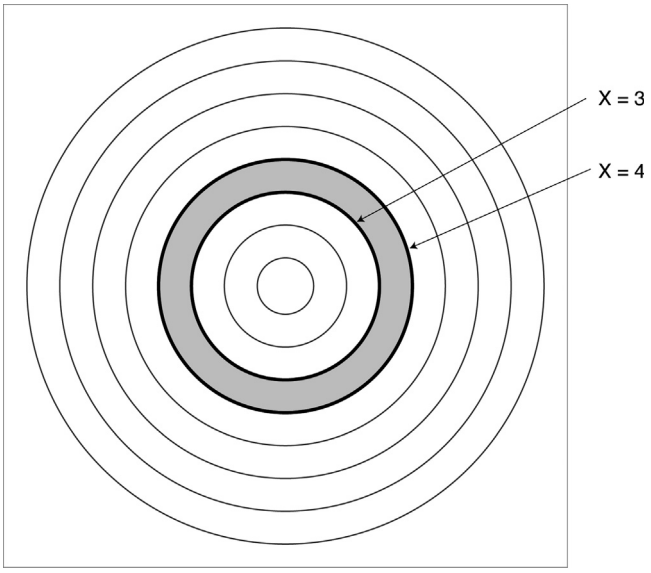

Fig. 3. Scheme of concentric rings based features calculation for $N=8$. On the step 4 average intensity of all pixels between circles $X=3$ and $X=4$ will be calculated.

Thereby the calculated features show both average intensity of an image as well as its decrement, depending on a distance from the image centre. The thickness of the rings, and, consequently, their amount, N, is a spatial resolution parameter.

Fig. 3 shows a scheme of calculating the features using $N=8$ rings. Thus, for $X=3$ intensity of all pixels between the 3rd and 4th circles will be averaged (grey area on the picture).

The two above described types of features were calculated for 15 images of every milk sample. Besides that, this radial averaging approach was also used for calculating features of HDR images, produced from every bracketing series.

2.4. Data analysis

Visual inspection of images and principal component analysis (PCA) [20] were preliminary used for exploring the images and calculated features.

Partial Least-Squares regression was used to build linear regression models for prediction of fat and protein content. Ring based features calculated for 16, 24, 32 and 48 rings were used as predictors in order to find optimal solution. The ring features were smoothed using Savitsky-Golay filter (filter width = 3 and polynomial order = 1), processed with Standard Normal Variate algorithm and mean centred.

Random repeated cross-validation with four segments and eight iterations was used for validating all PLS models shown in the present paper. In addition to traditional prediction performance indicators such as determination coefficient (R^2) and root mean squared error (RMSE), a ratio of standard error of cross-validated prediction (SECV) to sample standard deviation (RPD = SDy/SECV) was used to compare the obtained models [21].

The models were optimised by variable selection based on the competitive adaptive reweighted sampling (CARS) method. CARS improves regression models by selecting variables with large absolute regression coefficients [22]. Originally developed for dealing with spectra, it works well for any multivariate data with high collinearity.

The individual PLS models for protein and fat content prediction were built both separately on the respective set and for the joint set of 96 samples.

All calculations were carried out in MATLAB R2012a (Mathworks) supplemented with PLS_Toolbox v. 7.0 (Eigenvector Research Inc., Wenatchee, USA.).

3. Results and discussions

3.1. Visual inspection of images

On the first step, a visual inspection of the images with different fat and protein content taken for samples with or without homogenisation has been carried out (Fig. 4). An increase in protein and, particularly, in fat content results in a noticeable growth of sample optical density, and hence, lower general intensities and smaller sizes of observed light spots (Fig. 4a and b). It holds true for all three light sources, however, at some weaker differences for the red. The ultrasound treatment braking down the larger fat globules has similar effect on the images.

In all these cases, the observed growth of sample optical density is accounted for by growing scatter intensity due to the increasing particle number (or density) in a sample [10].

For the green light, these differences are clearly seen in the 3D representation of images shown in Fig. 5. Both spot sizes and their spatial profiles obviously depend on fat and protein content as well as on the homogenisation time. It can also be seen, that the effect of particle size on an image of the same sample (Fig. 5c) prevails over the effects of sample compositional variations (Fig. 5a and b).

3.2. Feature selection and regression analysis of individual sets

The modelling of *F*- and *P*-set individually performed in this section is advantageous for exploratory data analysis, to study the variability effects and to compare different approaches to feature selection from images.

Several feature selection techniques have been tried and compared in preliminary PLS regression modelling applied to individual *P*- and *F*-set. The best results were obtained with histogram-based selection and the method of concentric rings suggested in the present work (Section 2.3).

Distribution histograms were calculated for each photo and used as features, so the feature vector for each measurement included 256 intensities × 3 light sources × 5 exposition times =

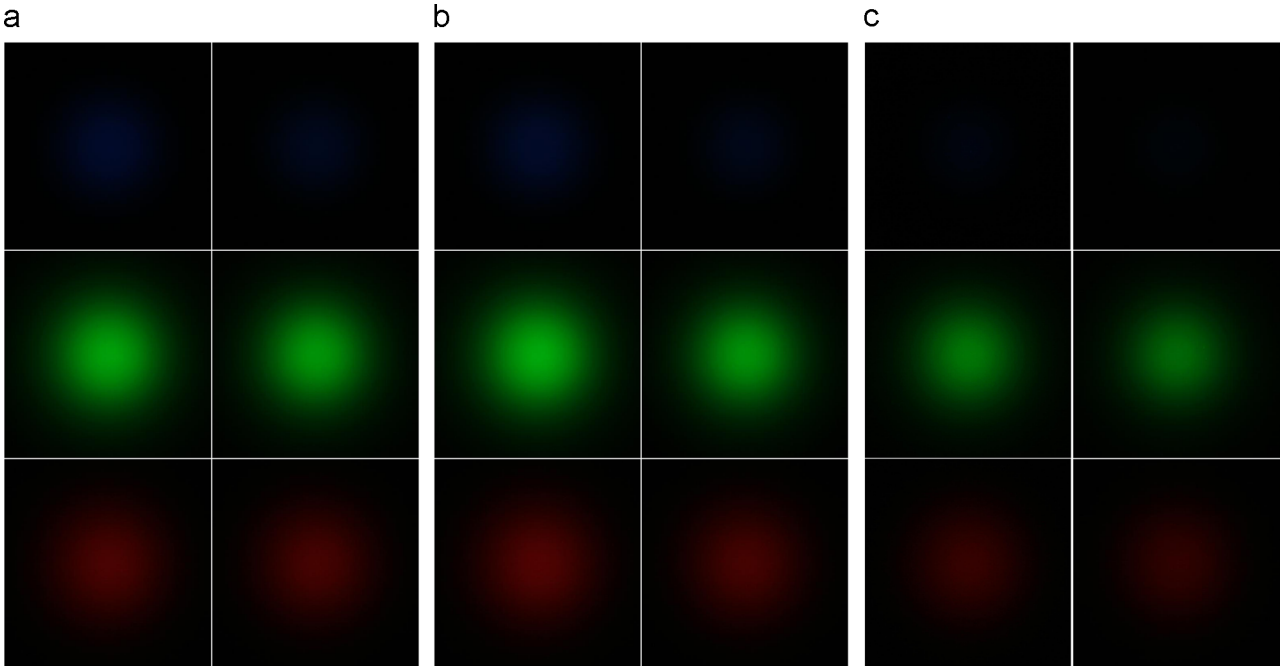

Fig. 4. Visual inspection of images for exposition time 1/4 s: (a)samples P1 (left) and P4 (right) without homogenisation, (b) samples F1 (left) and F4 (right) without homogenisation, (c) sample F4 after 10 s (left) and 20 s (right) of homogenisation.

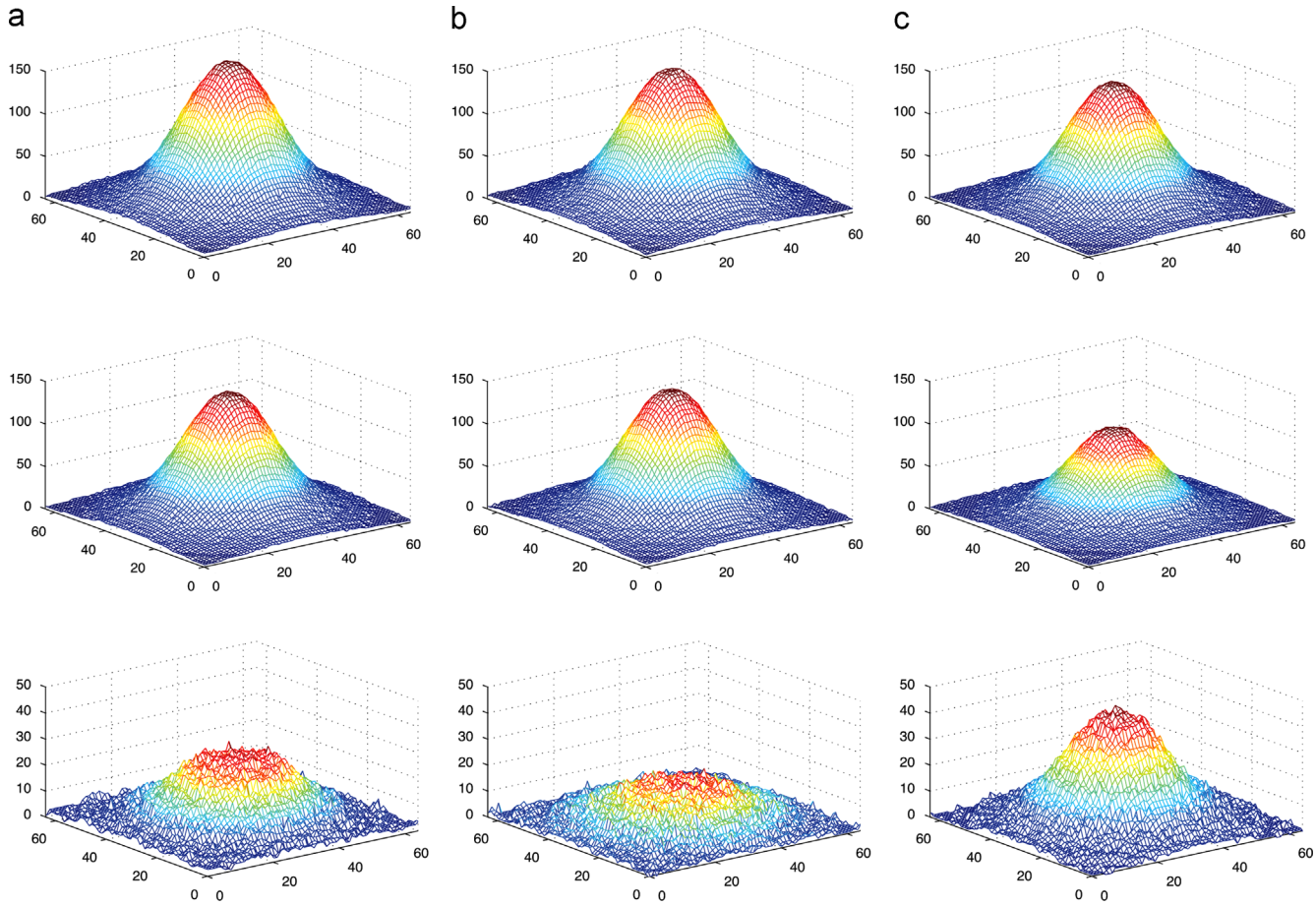

Fig. 5. 3D representation of green light intensity for exposition time 1/4 s: (a) samples F1 (top) and F4 (middle) and the difference between them (bottom), (b) samples P1 (top) and P4 (middle) as well as the difference between them (bottom), (c) sample F4 without homogenisation (top) and after 20 s of homogenisation (middle), the bottom image shows the difference. (For interpretation of the references to color in this figure legend, the reader is referred to the web version of this article.)

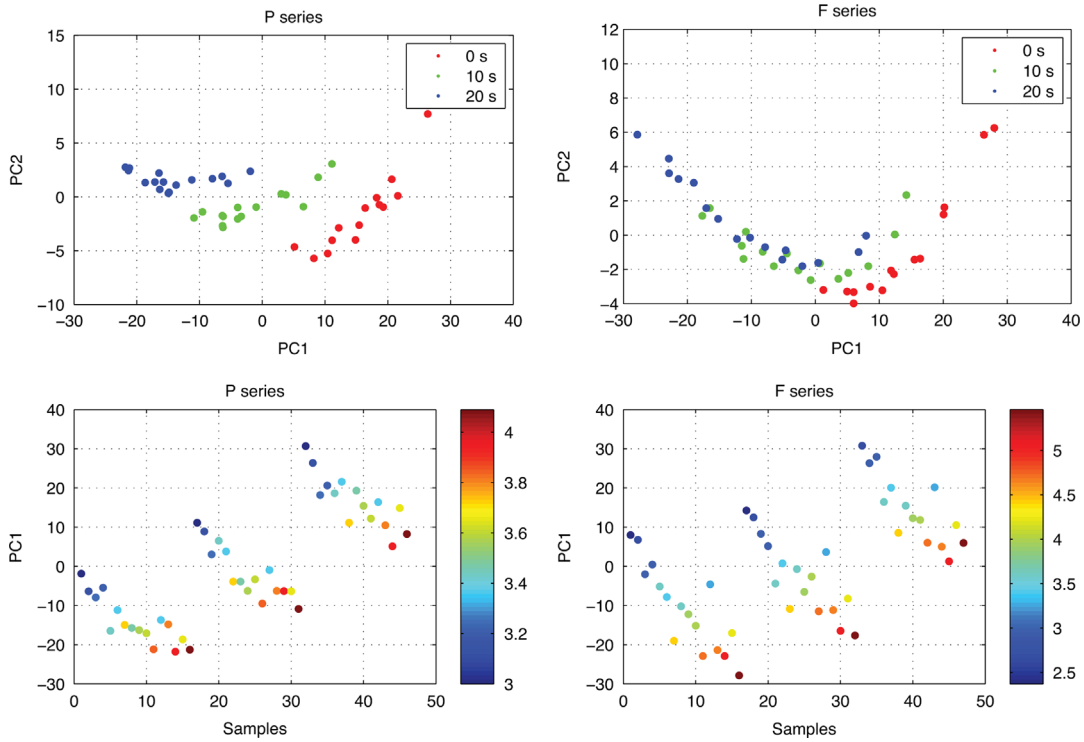

Fig. 6. PCA results for concentric rings based features for *P*-set (left) and *F*-set (right). On the top plots (PC1 vs. PC2) colour shows different homogenisation time. On the bottom plots (PC1 vs. sample number) a concentration of protein and fat are colour-coded. (For interpretation of the references to color in this figure legend, the reader is referred to the web version of this article.)

3840 values. The obtained PLS models were better for the prediction of total protein content ($R^2=0.88$) than fat ($R^2=0.81$), but both were far from the satisfactory values.

The advantage of suggested technique using concentric segments over other feature extraction methods could be expected, as the histogram features do not take spatial pixel arrangement into account.

To investigate the internal data structure of the concentric rings features, PCA was performed on *F*- and *P*-set of samples. PCA results for features, calculated using 16 rings, are shown in the Fig. 6. It is clear that the first two PCs describe both homogenisation degree (in particular, PC1) and sample composition, i.e. fat (for *F*-set) and total protein (for *P*-set) content. The first PC is therefore responsible for the total density of scattering particles in a sample. This observation is in good agreement with the results of visual data inspection given above and with previous spectroscopic study of similar data [8].

Table 2
PLS modelling and statistics for cross-validated predictions for fat content in *F*-set.

Type	nLV	RMSECV	RPD	R^2
48 seg, CARS varsel	3	0.147	6.083	0.973
48 seg, no varsel	5	0.216	4.150	0.944
48 seg, HDR, CARS carsel	4	0.211	4.123	0.943
48 seg, HDR, no varsel	5	0.331	2.571	0.862

Table 3
PLS modelling and statistics for cross-validated predictions for protein content in *P*-set.

Type	nLV	RMSECV	RPD	R2
48 seg, CARS varsel	3	0.049	6.147	0.974
48 seg, no varsel	4	0.072	4.150	0.944
48 seg, HDR, CARS varsel	4	0.063	4.617	0.954
48 seg, HDR no varsel	4	0.091	3.290	0.911

The results for PLS regression on concentric ring features are shown in Tables 2 and 3. The number of rings was found to have a minor influence to the model performance, final (best) models were obtained using 48 rings. Thus, the best model for prediction of fat in *F*-set had determination coefficient for cross-validated samples 0.973 with 3 latent variables (RMSECV=0.147). Prediction of protein content for *P*-set was comparable both with original data as well as after variable selection giving cross-validated predictions with $R^2=0.97$ with 3 latent variables (RMSECV=0.049). Using HDR images did not improve the results; in general all models built for HDR images had slightly worse prediction performance.

In all cases using CARS for variable selection allowed to get models with better predictions. Predicted vs. measured and RMSE plots for the best models with and without variable selection are shown in Fig. 7 for *F*-set and in Fig. 8 for *P*-set.

3.3. Joint data analysis

On the next step the proposed modelling method has been applied for joint analysis of the whole dataset including 96 measurements. Combining two sets of *F*- and *P*-samples eliminates some correlation between fat and protein (residual $r=0.03$) existing in initial standards [8], and thus, provides a realistic estimation of the model performances.

Preliminary investigation has brought similar results for the optimal number of rings in the feature selection algorithm as for the individual (Section 3.2). Therefore, the concentric ring algorithm with 48 rings was applied prior to the modelling. The PCA scores plots looked very similar to the one made for individual *F*-set.

The results of PLS-regression for prediction of each of the quality parameters with and without variable selection are shown in Table 4, the corresponding predictions plots are presented in Fig. 9. An obvious drop in prediction performance was discovered for fat (cross-validated $R^2=0.890$ vs. 0.973 for individual *F*-set) and especially for protein (cross-validated $R^2=0.724$ vs. 0.974 for individual *P*-set) content. Variable selection led to some minor

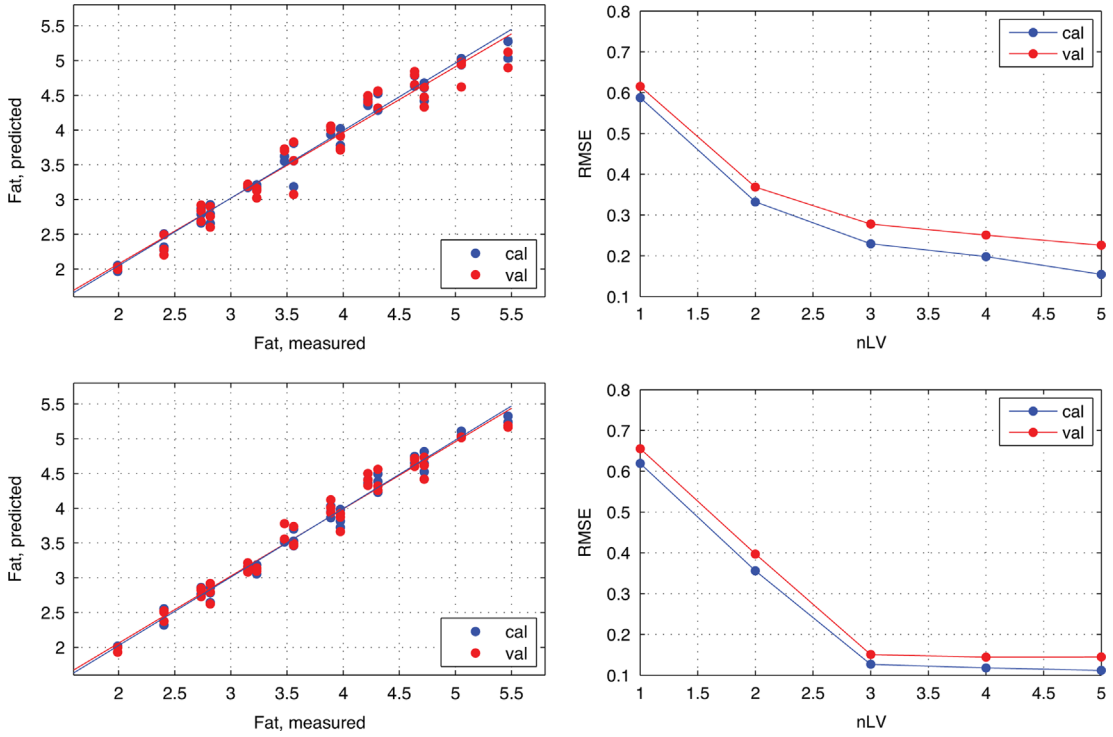

Fig. 7. PLS regression results on concentric rings based features prediction of fat in *F* set (top—with original data; bottom—after CARS selection of variables).

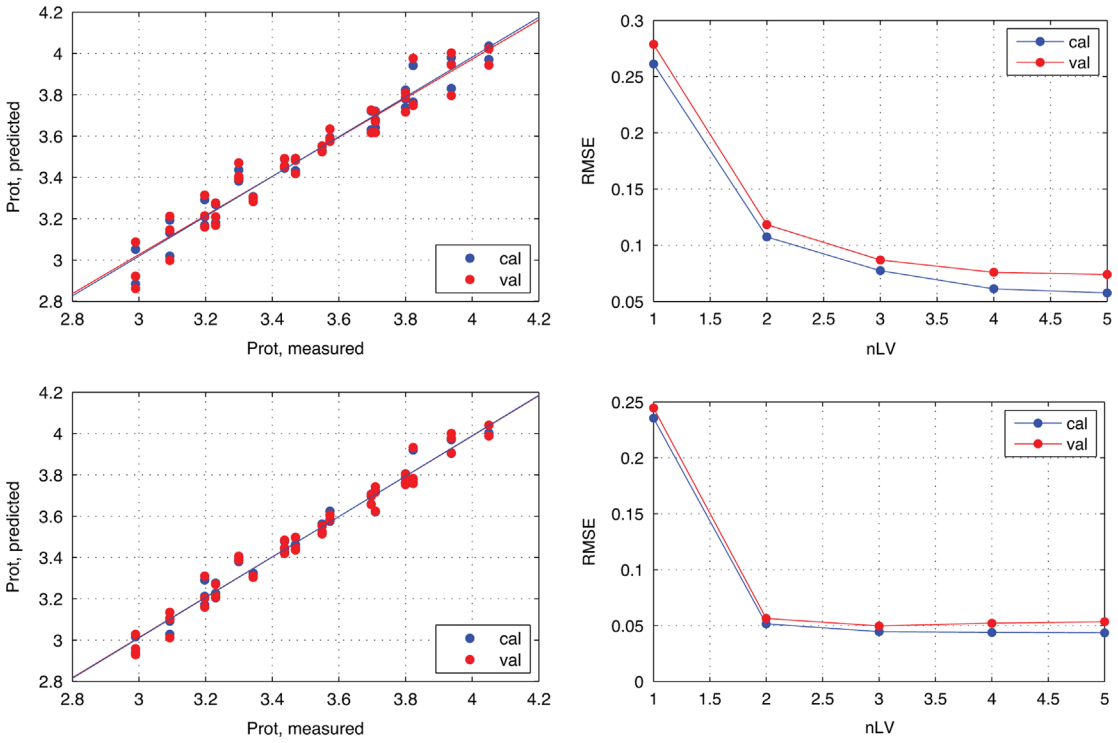

Fig. 8. PLS regression results on concentric rings based features for prediction of protein in *P* set (top—with original data; bottom—after CARS selection of variables).

Table 4
PLS modelling and statistics for cross-validated predictions for the joint set.

Type	nLV	RMSECV	RPD	R2
Fat, no varsel	6	0.251	2.415	0.852
Fat, CARS varsel	4	0.215	2.882	0.890
Prot, no varsel	6	0.148	1.294	0.595
Prot, CARS varsel	5	0.122	1.670	0.723

improvements in prediction performance and reduced the number of latent variables.

3.4. Discussion

Pixel intensity on a milk sample image depends on size and density of scattering fat and protein particles, and consequently, on their content. At the same time, the detected intensity depends on a pixel position with regard to the light source (i.e. the angle) and on the wavelengths. The efficient feature extraction method proposed in this paper was able to capture and emphasise both spectral and spatial differences between individual pixels.

The performances of models built for *P*- and *F*-set (Tables 2 and 3) individually are noticeably higher than in the joint model (Table 4), but lower than in the spectroscopic analysis in the region 400–1100 nm [8], where RMSECV=0.08 and 0.04 were reported for fat and total protein, respectively. Similar measurement geometry (diffuse transmission through a milk layer of about 4 mm) and identical experimental design allow interpreting the difference between the present method and spectroscopic analysis as a result of technical simplification. Spectral region in the present method is squeezed to about 200 nm (Fig. 1) against 700 nm range in the spectroscopic method; and hundreds of spectral variables are replaced with three broad band channels. Considering this dramatic reduction of spectral information content the resulting performance loss was absolutely expected. Although some gain is definitely obtained from using space-resolve image information (compare the histogram and ring-based feature selection methods), it has not been decisive here. Nevertheless, the accuracies offered by the suggested imaging method are absolutely acceptable for a quick and inexpensive analytical technique like this.

The present new technique has essential sensitivity to the scatter-driven effects on an image. At the same time, the deficiency of spectral information, e.g. minor components' absorbance that is generally observed below 450 nm and above 900 nm, makes the analysis in the whole sample variability range, provided by the present experimental design, challenging. This information deficiency can straightforwardly explain the joint model performance reduction compared to individual techniques (although the reference spectroscopic method was capable of handling this perfectly). Partially, it can be related to the presence of soluble proteins that do not scatter and thus stay invisible for the imaging, while due to the absorption in SW-NIR region can be detected and "factorised" by the PLS-regression model in case of full spectroscopic data. In this situation, the observed model deterioration could be caused by a difference in whey protein content between *F*- and *P*-set (which is very likely, considering that skim milk powder can be added by the standard preparation technology [8]). Another observation indirectly confirming the negative role of *P*-samples with artificially enhanced protein content can be made when studying Fig. 9. These samples taking middle position in the fat concentration range on predicted vs. reference plot exhibit noticeably higher prediction errors than *F*-set. Similar effect from other minor components cannot also be excluded.

The prediction accuracy of protein content for individual set is high (R^2=0.974/0.944, 3/5 LVs); it is closer to the results of spectroscopic analysis [8]. In this case, similar statistics of fat content prediction (R^2=0.973/0.944, 3/5 LVs) look confusing at a first glance, considering stronger effect of fat content on the image intensity (Fig. 5). Worse performance of the fat model compared to the spectroscopic method [8] can be explained, in addition to the above considerations, by close similarity of two effects: fat content enhancement and ultrasound treatment, both leading to the growth in fat globule density in a sample, and consequently, to higher scatter intensity. In the case of spectroscopy PLS regression

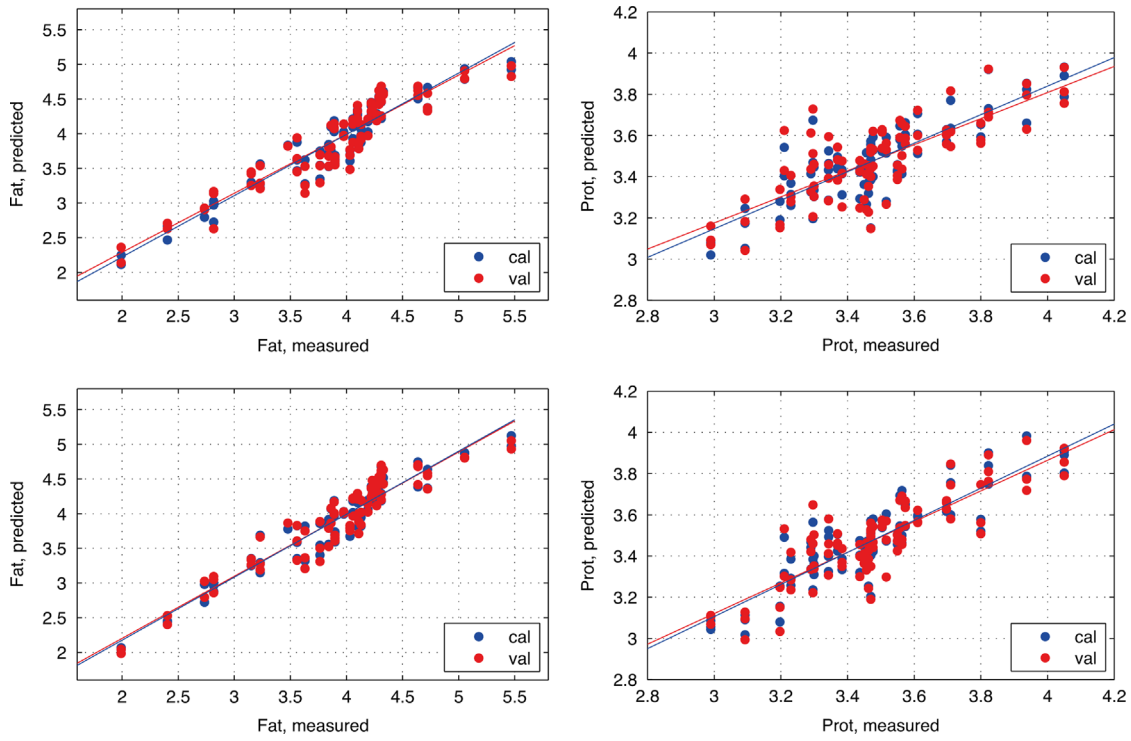

Fig. 9. PLS regression results on concentric rings based features for prediction of protein (left) and fat (right) in the joint set of samples (top—with original data; bottom—after CARS selection of variables).

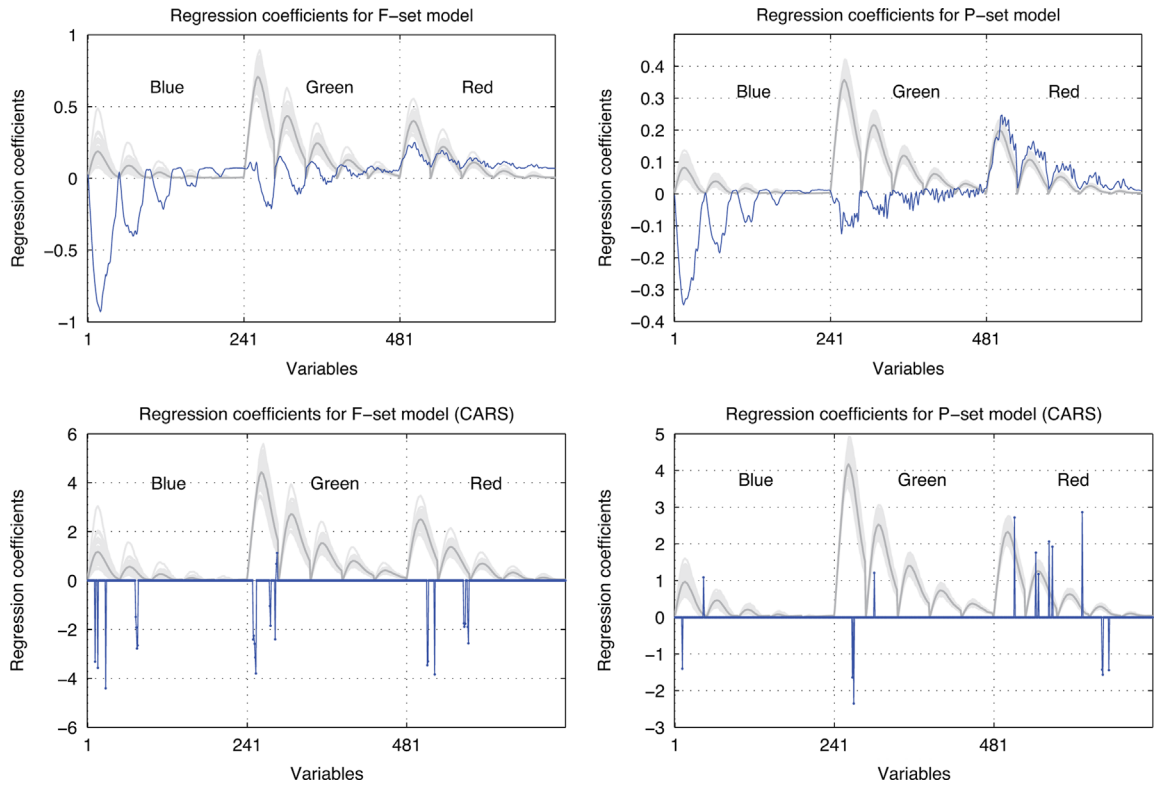

Fig. 10. Regression coefficients for F-set (left) and P-set (right) before and after variable selection (grey lines show rescaled original variables).

successfully handles this situation [8] by distinguishing those effects by their full-range spectral patterns. Perhaps, in the present method this similarity presents a more serious complication. At the same time, the applied homogenisation is known to have little or no effect on the protein micelles, and hence, it does not affect the performance of total protein models.

Correlation between fat and protein content is quite common for milk and it can be further enhanced in the standards due to

their preparation methods [8]. This correlation was noteceable for the *P*-set (0.72) and moderate for the *F*-set (−0.47), in any case, much lower than predicted vs. reference correlation. So it can be assumed that the models are casual, rather than based on indirect spurious correlations (i.e. if the method were sensitive to one component only and predicted the other one because of their correlation). Investigation of the regression coefficients for the best models showed that despite obvious similarity (Fig. 10), there is a difference, e.g. red channel seems to be more important for prediction of protein. This conclusion is also confirmed by the variables selected for each set (Fig. 10). Therefore, existing fat and protein correlation in individual sample sets should not be considered as the main reason of their better performance in the modelling.

Another minor complication was caused by outliers. In this study there were from two to four samples that had large Q^2 residuals (squared distance from a sample to latent variable space) and/or high leverage (squared distance from projection of sample to latent variable space to the origin of the space). Inspecting photos from these samples showed the presence of air bubbles in the milk, which, in spite of great efforts removing them before measurements, sometimes remained causing significant difference in features. Thus, for the future modelling, it is important avoiding the bubbles as well as other artefacts before taking photos is one of technical and modelling problems to be solved in the future method development and its transformation onto a measuring device.

4. Conclusions

The capability of accurate prediction of fat and total protein content in raw milk from conventional digital images in the presence of significant variability of compositions and particle sizes is the most valuable result of this study. Although the model performances are worse than in a physically similar scatter-based method using Vis/SW-NIR spectroscopy [8], the present results are of high practical significance, considering the technical simplicity of suggested technique. This approach can be utilised for the development of compact and inexpensive analysers of raw milk quality, in particular, for in-line or field measurement.

References

[1] R. Tsenkova, S. Atanassova, K. Toyoda, Y. Ozaki, K. Itoh, T. Fearn, J. Dairy Sci. 82 (1999) 2344–2351.
[2] P. Walstra, J. Dairy Sci. 50 (1967) 1839–1840.
[3] U.S. Ashworth, J. Dairy Sci. 52 (1969) 262–263.
[4] Q. Xin, H. Zhi Ling, T. Jian Long, Y. Zhu, Opt. Lasers Eng. 44 (2006) 858–869.
[5] Åsmund Rinnan, F. van den Berg, S.B. Engelsen, Trends Anal. Chem. 28 (2009) 1201–1222.
[6] M. Rocío, M.A. Pérez, C. de la Torre, C.E. Carleos, N. Corral, J.A. Baro, in: XIX IMEKO World Congress Fundamental and Applied Metrology, Lisbon, Portugal, 2009, pp. 2564–2568.
[7] C.L. Crofcheck, F.A. Payne, C.L. Hicks, M.P. Menguc, S.E. Nokes, J. Food Process Eng. 23 (2000) 163–175.
[8] A. Bogomolov, A. Melenteva, Chemom. Intell. Lab Syst. 126 (2013) 129–139.
[9] A. Bogomolov, S. Dietrich, B. Boldrini, R.W. Kessler, Food Chem. 134 (2012) 412–418.
[10] A. Bogomolov, A. Melenteva, D. Dahm, J. Near Infrared Spectrosc. 21 (2013) 435–440.
[11] S. Kucheryavski, K.H. Esbensen, A. Bogomolov, J. Chemom. 24 (2010) 472–480.
[12] S. Kucheryavski, Chemom. Intell. Lab. Syst. 108 (2011) 2–12.
[13] M.H. Bharati, J. Jay Liu, J.F. MacGregor, Chemom. Intell. Lab Syst. 72 (2004) 57–71.
[14] P.W. de Bont, G.M.P. van Kempen, R. Vreeker, Food Hydrocoll. 16 (2002) 127–138.
[15] N. Fucà, C. Pasta, G. Impoco, M. Caccamo, G. Licitra, Int. Dairy J. (2012).
[16] I. Scherze, R. Knofel, G. Muschiolik, Food Hydrocoll. 19 (2005) 617–624.
[17] J.R. Frisvad, N.J. Christensen, H.W. Jensen, ACM Trans. Graph 26 (2007) 60.
[18] B. Aernouts, E. Polshin, J. Lammertyn, W. Saeys, J. Dairy Sci. 94 (2011) 5315–5329.
[19] E. Reinhard, G. Ward, S. Pattanaik, P. Debevec, High Dynamic Range Imaging: Acquisition, Display, and Image-Based Lighting, 1st ed., Morgan Kaufmann, San Francisco, CA, USA, 2005.
[20] K.H. Esbensen, P. Geladi, in: E.-C.S.D. Brown, R. Tauler, Beata Walczak (Eds.), Comprehensive Chemometrics, Elsevier, Oxford, 2009, pp. 211–226.
[21] P. Williams, D. Sobering, J. Near Infrared Spectrosc. 1 (1993) 25.
[22] H. Li, Y. Liang, Q. Xu, D. Cao, Anal. Chim. Acta 648 (2009) 77–84.